Transparent Nanopaper-Based Flexible Organic Thin-Film Transistor Array

Yoshihide Fujisaki, Hirotaka Koga, Yoshiki Nakajima, Mitsuru Nakata, Hiroshi Tsuji, Toshihiro Yamamoto, Taiichiro Kurita, Masaya Nogi, and Naoki Shimidzu*

Eco-friendly and low-cost cellulose nanofiber paper (nanopaper) is a promising candidate as a novel substrate for flexible electron device applications. Here, a thin transparent nanopaper-based high-mobility organic thin-film transistor (OTFT) array is demonstrated for the first time. Nanopaper made from only native wood cellulose nanofibers has excellent thermal stability (>180 °C) and chemical durability, and a low coefficient of thermal expansion (CTE: 5–10 ppm K^{-1}). These features make it possible to build an OTFT array on nanopaper using a similar process to that for an array on conventional glass. A short-channel bottom-contact OTFT is successfully fabricated on the nanopaper by a lithographic and solution-based process. Owing to the smoothness of the cast-coated nanopaper surface, a solution processed organic semiconductor film on the nanopaper comprises large crystalline domains with a size of approximately 50–100 μm, and the corresponding TFT exhibits a high hole mobility of up to 1 $cm^2 V^{-1} s^{-1}$ and a small hysteresis of below 0.1 V under ambient conditions. The nanopaper-based OTFT also had excellent flexibility and can be formed into an arbitrary shape. These combined technologies of low-cost and eco-friendly paper substrates and solution-based organic TFTs are promising for use in future flexible electronics application such as flexible displays and sensors.

1. Introduction

The outstanding features of flexible displays such as excellent mechanical flexibility, a light weight, and shock resistance are expected to enable a wide range of applications in the display field, such as mobile terminals, arbitrary-shaped digital signage, and large-area sheet-type displays. In recent years, the research and development of flexible displays using plastic substrates as a more durable and lightweight alternative to rigid glass has been promoted actively, and various types of displays based on liquid crystals, organic light-emitting diodes, and electronic paper have been reported.[1–4] However, the low thermal durability and high coefficient of thermal expansion (CTE) of plastic substrates frequently become a major obstacle in the manufacturing process. High-quality plastics that can alleviate these problems are expensive. Because the substrate occupies a large part of display devices, cost-effective and environmentally friendly materials are strongly required. Paper, made from natural wood resources, i.e. cellulose, is ubiquitous in society, and is an attractive potential material for substrates.[5] In fact, in recent years, flexible electronics based on paper have attracted considerable attention as a possible next-generation technology to replace currently used plastic-based electronics. A wide range of applications such as smart pixels,[6] memory devices,[7] printed circuits,[8] electrowetting,[9] batteries,[10] photovoltaic devices,[11] and touch sensors[12] have been demonstrated on substrates made of conventional paper. If we can use cheap and naturally derived paper as substrates for displays, it will have a significant impact on the display industry from the viewpoints of reduced cost and environmental impact.

Active devices such as thin-film transistors (TFTs) are indispensable components for the low-power-consumption driving of displays.[13] To realize large-area and high-resolution displays on paper, electrical performances either equaling or surpassing those of conventional amorphous Si TFTs, for example, mobility over 1 $cm^2 V^{-1} s^{-1}$, and a current on/off ratio over 10^6, will be required.[14] In recent years, a great deal of effort has been made to fabricate various types of TFTs on paper such as those based on amorphous oxide semiconductors.[15,16] A complementary metal oxide semiconductor inverter circuit has also been demonstrated.[17] In contrast to inorganic or metal-oxide-based TFTs, organic thin-film transistors (OTFTs) have many technical merits such as low-temperature deposition, large-area production, and a solution-based process.[18] These desirable features make OTFTs an ideal candidate for active devices on paper substrates. In addition, the highly bendable structure of organic components originating from van der Waals bonding also make them compatible for use with highly flexible paper substrates. Previously, some research groups have demonstrated polymer

Dr. Y. Fujisaki, Dr. Y. Nakajima, Dr. M. Nakata, Dr. H. Tsuji, T. Yamamoto, Dr. T. Kurita, Dr. N. Shimidzu
Japan Broadcasting Corporation (NHK)
Science and Technology Research Laboratories
1–10–11, Kinuta, Setagaya-ku, Tokyo, 157–8510, Japan
E-mail: fujisaki.y-hu@nhk.or.jp
Dr. H. Koga, Dr. M. Nogi
The Institute of Scientific and Industrial Research
Osaka University
8–1 Mihogaoka, Ibaraki, Osaka, 567–0047, Japan

DOI: 10.1002/adfm.201303024

or vapor-deposited small-molecule-based OTFTs on paper or banknotes.[19–21] However, the device performances were generally inferior to those of devices on glass or plastic substrates owing to the limitation imposed on the process temperature and the large surface roughness of the paper. More recently, to increase mobility, a solution-processed organic semiconductor material has also been used in a device on paper.[22] However, while many studies have focused on enhancing the performances of TFTs, there have been few reports focused on improving paper substrates to enable high-performance device integration. Most of the demonstrations have used commercially available coated white paper. However, the coated paper has poor chemical and thermal durability owing to its coated layers, making it difficult to fabricate high-resolution TFT arrays using versatile integration processes such as photolithography and etching. Furthermore, considering applications to transmissive- or emissive-type displays, optically transparent paper is desirable for constructing high-resolution TFT arrays. Thus, the realization of high-mobility OTFTs using transparent paper substrates that can withstand a versatile integration process is still a major challenge regarding paper-based flexible electronics applications.

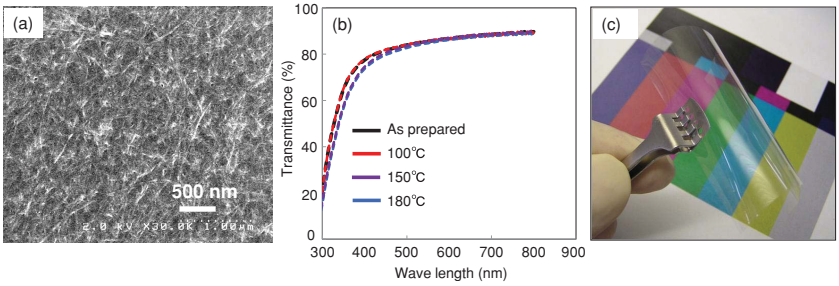

Figure 1. a) SEM image of fabricated nanopaper. The scale bar is 500 nm. b) Optical transmittance of nanopaper for different curing temperatures. The nanopaper exhibited excellent transmittance of 83% after 180 °C curing. c) Photograph of 20-μm-thick transparent cellulose nanofibers paper after 180 °C curing. The nanopaper exhibited excellent transparency.

In this work, we report the development of high-mobility organic TFT arrays on thin transparent paper. A 20-μm-thick transparent paper, which was made from only native wood cellulose nanofibers,[23] was applied to the integration process of an OTFT array for the first time. High thermal durability at over 180 °C, a low CTE, and excellent resistance to solvent attack, which originate from the native crystalline cellulose, allowed us to fabricate devices in a manner similar to those on glass or high-quality plastic. Moreover, we fabricated both the nanopaper and the OTFT array using solution-based techniques suitable for large-area and low-cost production. The fabricated short-channel OTFT exhibited a high mobility of up to 1 $cm^2 V^{-1} s^{-1}$, good air-stability and a mechanically flexible structure.

2. Results and Discussion

To realize a high-performance OTFT array for flexible displays, highly optically transparent substrates compatible with glass substrates are desired. We fabricated optically transparent substrates using cellulose nanofibers (see Supporting Information, Figure S1). In our procedures, the pulp was isolated into 15-nm-wide cellulose nanofibers because they were subjected to repeated mechanical nanofibrillation. When such narrow cellulose nanofibers were cast onto a smooth acrylic substrate, the obtained paper exhibited a much smoother surface than normal paper (Figure S1a,b, Supporting Information). Moreover, cellulose nanofibers tend to collapse by capillary action during the evaporation of water, and the deformed condition is fixed by hydrogen bonds that form between hydroxyl groups of the cellulose. As a result, the interstices between the nanofibers are sufficiently small to avoid light scattering in the dried cellulose nanofiber sheets as shown in the scanning electron microscopy (SEM) image of **Figure 1**a. The precise procedures used in the nanofibrillation of wood pulp and the fabrication of paper substrates impart high optical transparency to the nanopaper. The obtained smooth surface not only improves the transparency of the nanopaper but is also beneficial for the deposition of the thin multilayer structure of the OTFT array.

In addition to optical transparency, a low CTE is a critical requirement for the substrate. Flexible displays for moving pictures generally require TFTs with shorter channel length L below 10 μm to obtain a larger drain current, which is responsible for controlling pixels at a high frame rate of over 60 Hz and to obtain high brightness. When high-resolution TFT arrays are fabricated on substrates, undesirable thermal warping and shrinkage of the substrates may occur during the heating process. Therefore, glass substrates with a low CTE are suitable, although they have low flexibility. Although plastics have been widely studied, most of them have a large CTE (approx. 50 ppm K^{-1}), and foldable plastics exhibit particularly extremely large CTEs in excess of 200 ppm K^{-1}. Cellulose nanofiber sheets consist of only cellulose nanofibers, which have a low CTE of 0.1 ppm K^{-1}, as low as that of quartz glass. As a result, the fabricated nanopaper had an extremely low CTE of 5–10 ppm K^{-1}, similar to that of glass.

High thermal durability is also an important requirement of substrates. To display moving pictures with a high response speed, high mobility is also required. Enhancement of the electrical performances of TFTs strongly depends on the film quality of the gate dielectric and the organic semiconductor (OSC) layer. For example, imperfect curing of the dielectric layer or insufficient vaporization of the organic solvent used for the OSC leads to unstable and deteriorated electrical performance owing to the residual solvent, ions, and moisture.[24] Therefore, polymer substrates or chemically modified cellulose nanofiber sheets with low thermal durability result in much lower TFT mobility than those on rigid glass substrates.[25] Figure 1b shows the optical transmittance of our nanopaper for various curing temperatures. TEMPO-mediated oxidation deteriorate the thermal durability of cellulose.[26] However, as the graph indicates, the fabricated nanopaper made from native cellulose nanofibers showed superior thermal durability to chemically modified nanocellulose substrates and maintained its transparency without brown discoloration even after curing at 180 °C for 1 h in air. After heating, the nanopaper has a high transmittance of 85.4% at 600 nm, which is almost the same

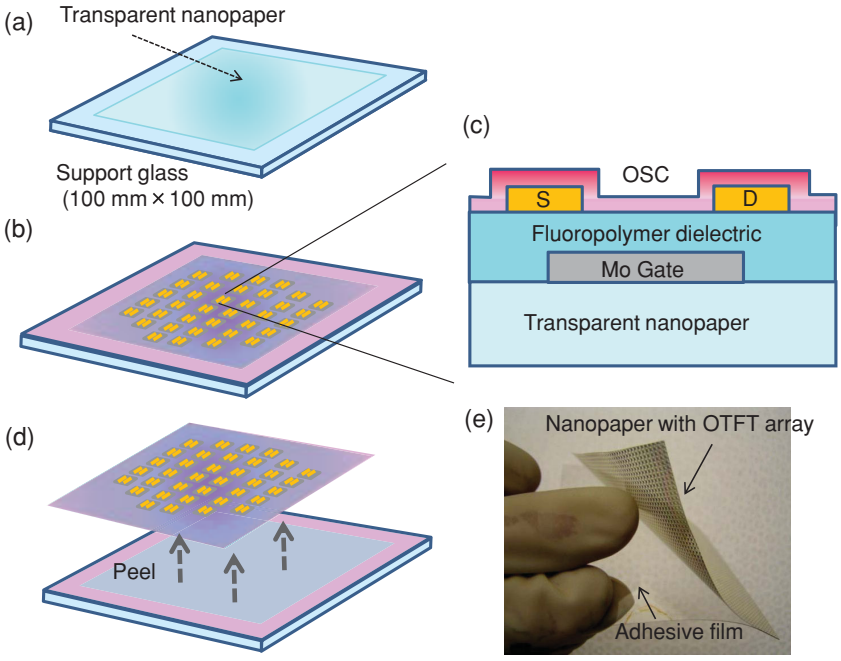

Figure 2. Schematic illustration of fabrication process for nanopaper-based bottom-contact OTFT array. a) A 20-µm-thick nanopaper is laminated on support glass using a temporary weak adhesive film. b,c) Schematic illustration and cross section of fabricated OTFT. d,e) The fabricated nanopaper-based OTFT array can be easily peeled off from support glass without any fracturing or cracks.

as the initial transmittance of 86.7%. Figure 1c shows a photograph of our transparent nanopaper after curing at 180 °C. The nanopaper consisting of native cellulose fibers also has high chemical resistance to common solvents such as acetone, acidic metal etchants, and resist developers, making it advantageous for fabricating bottom-contact OTFTs which suited for shrinking channel size. As mentioned above, the integration process of the OTFT array can be applied in a manner similar to that used for OTFT arrays on a conventional glass substrate.

Figure 2 shows a schematic illustration of the fabrication process and the cross-section structure of the bottom-contact OTFT array on a nanopaper. Photographs of the fabrication scheme are also shown in Figure S2, Supporting Information. To accomplish the process without floating or deformation of the thin nanopaper, a lamination and peel-off scheme was used. As shown in Figure 2a, we first laminated the nanopaper sheet on support glass using a temporary weak adhesive film. Prior to OTFT fabrication, the nanopaper was covered with a 2-µm-thick thermally cross-linkable olefin-type polymer[27] to enhance the mechanical flexibility of the device and to further planarize the surface of the nanopaper. The bottom-contact OTFT array based on fluoropolymer gate dielectric and a soluble small-molecule OSC was fabricated using a lithographic and solution-based process (Figure 2b,c). After the integration of the device, the 20-µm-thick transparent nanopaper was peeled off from the support glass without any fracturing or cracks (Figure 2d,e). **Figure 3**a shows a photograph of the fabricated transparent nanopaper-based OTFT array. A short-channel TFT arrays with a resolution of 70 × 70 was successfully integrated on the nanopaper. As shown in Figure 3b,c, the thin nanopaper-based structure provides a excellent flexibility and mechanical durability; thus, we can bend and fold the device without tearing or fracturing it similarly to conventional paper.

Optical microscopy images of the fabricated TFT array structure on the nanopaper and magnified images are shown in **Figure 4**a–c. In general, the height variation and morphology of metal and dielectric layers affect the insulating property. For example, the rough surface of the gate metal make it easy to induce pinholes or structual defects in the polymer dielectric layer, and this leads to a high leakage current. Moreover, the gate dielectric layer on the rough metal had an uneven surface, which deteriorated the adhesion of the S/D contact and contact resistance; therefore, TFTs exhibit deteriorated performance and a high leakage current. Thus, the uniform formation of several tens nm of each TFT components is very important. In this study, the metal contacts and gate dielectric layer deposited on the nanopaper had a flat surface and good uniformity of the thickness because of the smooth surface of the nanopaper. Figure 4d shows an atomic force microscopy (AFM) topography image of the gate dielectric layer on the nanopaper. From the topography image, we found that the gate dielectric layer was very smooth and the root mean square (RMS) roughness was 1.9 nm over an area of 20 µm × 20 µm. As a result, we obtained an acceptably low leakage current for the dielectric layer of below 10^{-8} A cm^{-2} at an applied voltage of 50 V (Figure 4e).

The formation of large crystalline domains in the OSC film is essential for high-mobility TFTs.[28–30] The crystalline structure of the OSC film strongly depends on the surface condition of the gate dielectric layer.[31,32] The properties of the interface between the OSC film and the dielectric layer also significantly affect the subthreshold slope, hysteresis, and trap density;[33,34] thus, the choice of the dielectric material is very

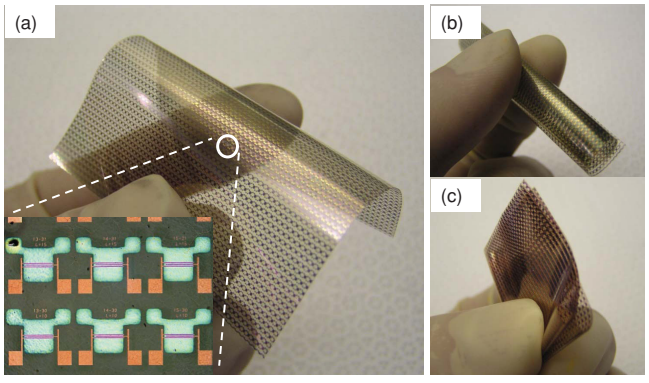

Figure 3. a) Photograph and optical microscopy image of 20-µm-thick transparent nanopaper-based OTFT array. Short-channel TFTs with a resolution of 70 × 70 were integrated in a 70 mm × 70 mm area. Photographs of OTFT array in b) bending and c) folding states.

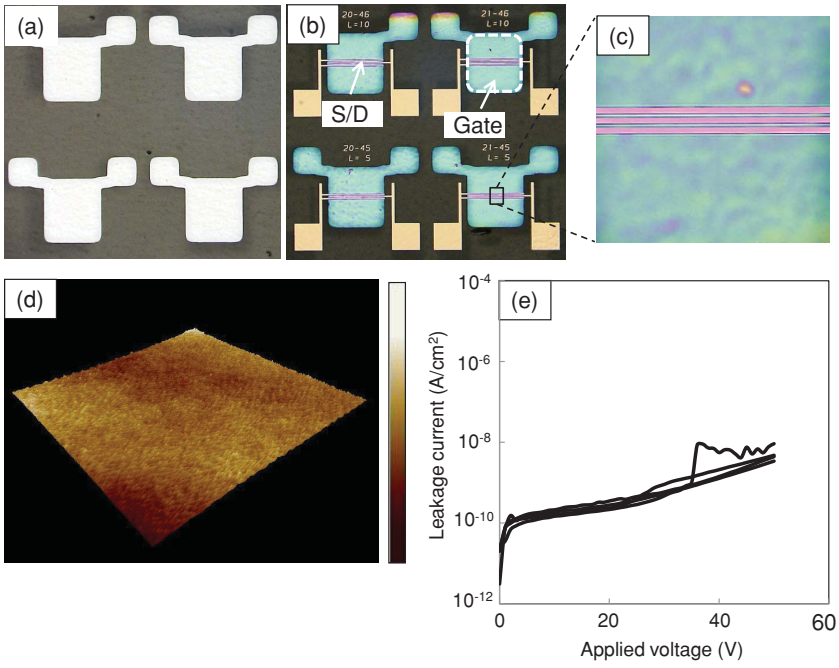

Figure 4. Optical microscopy images of OTFT array on nanopaper after a) gate metal patterning and b) S/D contact patterning. c) Magnified image of the channel region of the TFT. d) AFM topography image of spin-coated gate dielectric layer on nanopaper. The height scale is 12 nm. The surface roughness of the dielectric layer was estimated to be 1.9 nm. e) Leakage current of dielectric layer.

important. A gate dielectric with low surface energy is advantageous for controlling the molecular ordering and minimizing the number of interface traps. For example, an amorphous fluoropolymer such as Cytop or Teflon provides excellent TFT performance.[32,34,35] However, the strong dewettability of its hydrophobic surface often makes it difficult to deposit a solution-processed OSC film directly on the dielectric layer. In this study, we employed a hydroxyl-free partially fluorinated polymer dielectric (EPRIMA AL-X6, Asahi Glass, Japan). We optimized the solution wettability of the polymer by controlling the number of fluorinated alkyl groups at the dielectric surface to obtain wettability favorable for the organic solvent of the OSC. A 20 wt% propyleneglycol monomethylether acetate solution was spin-coated on the substrate and cured at 150 °C on a hot plate under air. In addition to the dielectric layer, the choice of an OSC material that provides good charge transport and reproducible processability is very important for achieving high mobility. Moreover, stable operation under ambient air is indispensable for practical applications. To this end, a soluble small-molecule OSC (lisiconS1200 Merck Chemicals Ltd.),[36] which has a low lying ionization potential (IP) of 5.4 eV, was employed in this work. We also used a mesitylene-based formulation which has a high boiling-point of 160 °C, as the solvent of the OSC solution to enable slow solvent evaporation during the spin-coating process. The measured water and meshitylene contact angles of the dielectric layer surface are shown in Figure S3, Supporting Information. Owing to the high solvent wettability of the dielectric surface, the OSC solution immediately spread out over the substrate after drop-casting. As a result, we obtained a uniform thin film by a simple spin-coating process. **Figure 5**a,b show optical microscopy and cross-polarized microscopy (CPM) images of the spin-coated OSC film on the nanopaper, respectively. We obtained large crystalline domains of size varying from 50 to 100 µm. For comparison, Figure 5c shows the crystalline structure of an OSC film on a glass substrate. In general, the crystalline structure of OSC films is severely affected at the atomic level by the surface roughness of the dielectric layer.[37] Owing to the smoothness of the nanopaper surface, the spin-coated OSC film exhibited a similar crystalline structure and crystalline domains with a similar size to those on the glass substrate. To further investigate the microstructure of the OSC film, we examined an atomic force microscopy (AFM) topography image of the film. As shown in Figure 5d, the OSC film exhibited a smooth terrace- and step-like morphology, and the step height of the discotic valleys was estimated to be approximately 2–3 nm from the height variation shown in Figure 5e.

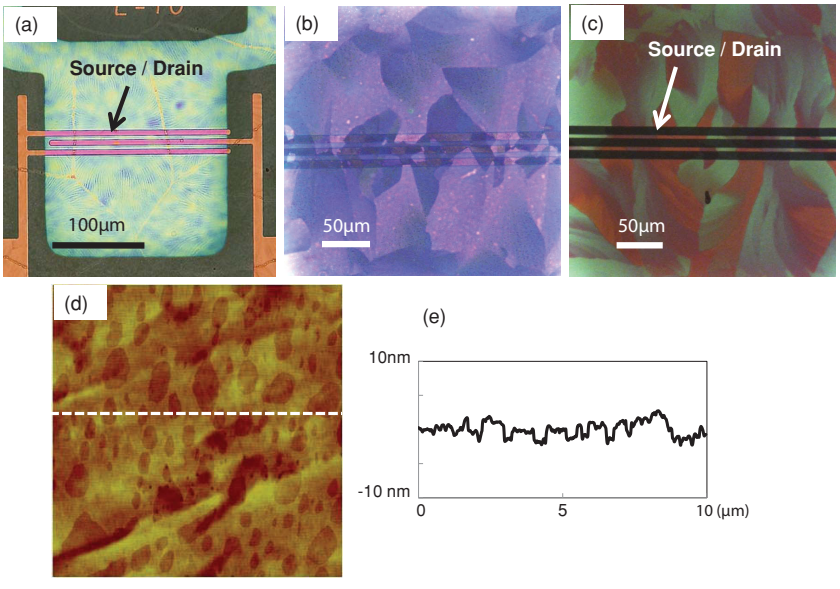

Figure 5. Magnified images of fabricated OTFT on transparent paper substrate. a) Optical microscopy image of the OSC film on nanopaper. Cross-polarized microscopy images of the OSC film on b) paper and c) glass substrates. d) Tapping-mode AFM image of OSC film on nanopaper and e) height variation along dashed line in (d).

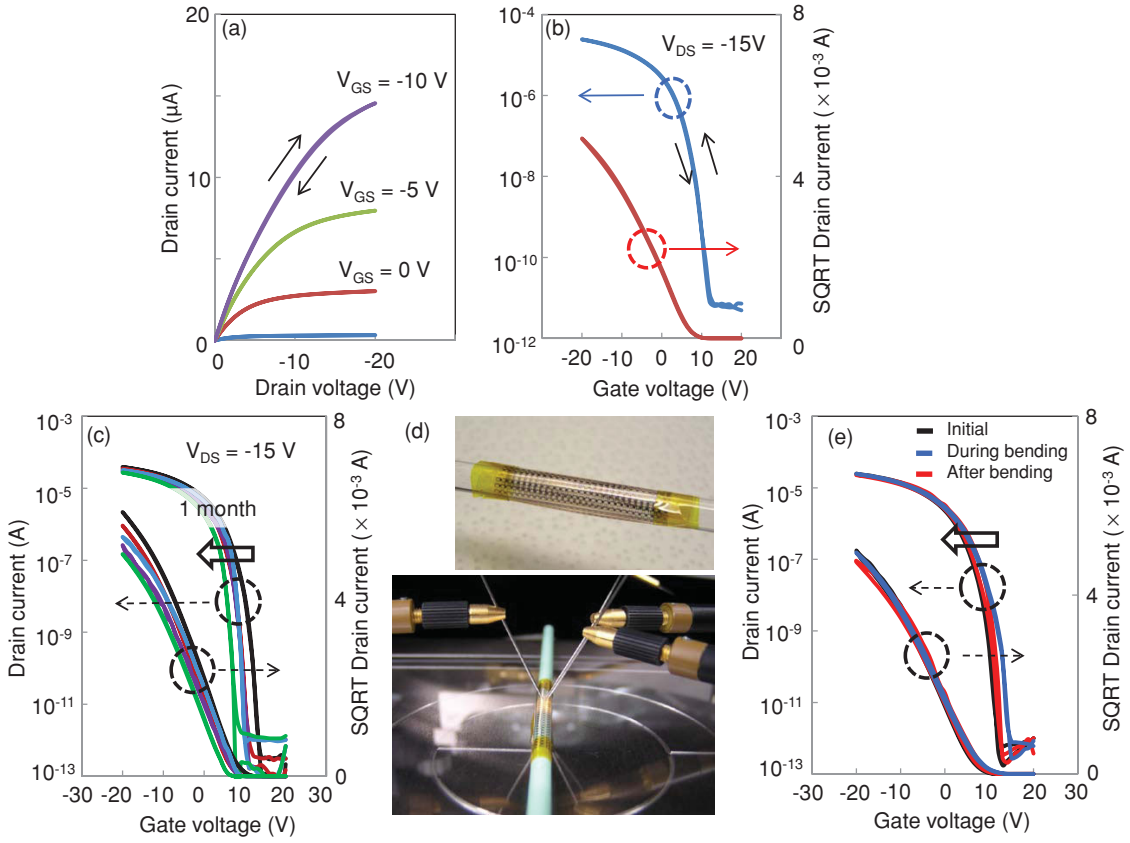

Figure 6. Typical electrical performances of fabricated OTFT array. a) Output and b) transfer characteristics measured under ambient air. Channel length is 10 μm. c) Transfer curves for different numbers of days exposed to air. d) Photographs of measurement approach for nanopaper-based TFT under bending. e) Measured transfer curves of TFTs before, during and after bending (black: initial; blue: during outward bending; red: after outward bending). Measurements were performed by wrapping the TFT array around a cylindrical bar with 2 mm diameter.

Figure 6a,b show plot of the typical output and transfer characteristics of the corresponding TFT on the nanopaper, respectively. The short-channel device with a channel length L of 10 μm exhibited a high on-current of over 10^{-5} A, a high on/off ratio of between 10^6 and 10^8, and its mobility reached 1 cm^2 V^{-1} s^{-1} under ambient air. We also obtained a small hysteresis of below 0.1 V and a relatively low subthreshold slope of 0.84 V per decade. These obtained characteristics indicate that the number of interface traps between the gate dielectric and the OSC film is very low.[27,33,38] The average mobility and subthreshold slope for 30 TFTs within a 5 cm × 5 cm area were 0.83 cm^2 V^{-1} s^{-1} and 1.1 V per decade, respectively (see Figure S4, Supporting Information). These results are similar to our previous results for a device with a plastic substrate.[27,39] This suggests that our device fabricated on the nanopaper has good interface quality similar to that of the device on the plastic substrate. We believe that the sufficient curing of both the dielectric and the OSC layer and the smooth surface of the nanopaper contributed to these results. The linearity at a low drain voltage in Figure 6a also indicates Ohmic-like carrier injection, which is attributed to the low injection barrier between the work function of the SAM-modified S/D contact and the HOMO energy of the OSC film. The energy level mismatch between the Fermi level of the SAM-treated Au contacts and the HOMO of the OSC film was measured to be 0.06 eV by photoelectron yield spectroscopy (Riken Keiki, AC-3). However, as shown in Figure S4 (Supporting Information), the fabricated array exhibited a range of characteristics and the mobility varied from 0.53 to 1.3 cm^2 V^{-1} s^{-1}. This variation is mainly due to the size variation of the crystalline structure (Figure S5, Supporting Information). The difference in grain boundary densities crossing the channel region determines the charge transport. Therefore, we consider that the formation of a larger crystalline domain or the control of the crystal size will be effective to decreasing the variation of the characteristics. Precise isolation of the OSC film will also effective to minimize the variation of on/off ratio which will cause crosstalk errors in the array device.

To evaluate the stability of the device in air, long-term stability was monitored during storage in air. Figure 6c shows the measured transfer curves as a function of the number of days of exposure to air. Despite the passivation layer, although a negative shift in the threshold voltage (V_{TH}) of 5 V and an approximately 13% reduction in mobility were observed, the fabricated TFT still exhibited a high mobility of 0.88 cm^2 V^{-1} s^{-1} and a small hysteresis of below 0.1 V after 1 month of storage in air. This is probably due to the high oxidation barrier of the OSC film with a deep IP and the dielectric interface with a low polar functionality.[40] This result suggests that the TFT on the nanopaper has good stability enough to maintain its high performance in the presence of moisture. The results for a 500 repeated cycling test after two months of storage in air

and constant gate bias stress are also plotted in Figure S6, Supporting Information. As can be seen from the figure, the fabricated TFT exhibited good stability. A relatively small V_{TH} shift of 1.8 V was observed after applying the gate stress for 10^4 s. As shown in Figure 6c, however, the large shift in V_{TH} indicates that long-term exposure to air induces charge trapping in the OSC or dielectric film. A shift in V_{TH} generally deteriaorate the luminance and causes image sticking on the display device; hence, the minimization of the shift is important for practical application. We consider that employing a passivation layer to protect the active layer from the penetration of oxygen and moisture is a promising approach to improving the stability in addition to the pretreatment process such as a nitrogen anneal. The moisture resistance of the cellulose paper can be improved by using various techniques, as previously reported.[41–44] The formation of an OSC film with a single-crystalline or larger crystalline structure will also suppress charge trapping at the dielectric interface and further improve the stability.[45] Finally, to evaluate the mechanical flexibility, we simply measured the bending stability by wrapping the TFT array around a cylindrical bar (2 mm diameter). Figure 6d shows photographs of measurement approach of the bending stability. Bending was performed in the parallel direction to the source-drain current path for 1 h. Figure 6e shows the transfer curves before, during, and after the outward bending of the substrate. Although a slight decrease in drain current and increase in hysteresis was observed, we found that the OTFT can still function and that no significant degradation of mobility occurred. Off-current remains below 1 pA, indicating that the leakage current through the gate dielectric layer is sufficiently low after the bending. In general, outward bending induce tensile strain to a device.[46,47] These results suggest that the thin nanopaper structure based on narrow cellulose nanofibers contributes to the excellent flexibility of the device and that the polymer planarization and dielectric layer also relax the bending-induced mechanical strain.

3. Conclusions

Transparent nano cellulose substrate attract considerable attensions for the application of flexible electron device.[48] In this study, a transparent nanopaper-based OTFT array was successfully demonstrated. Nanopaper made from only native cellulose nanofibers has high thermal and chemical durability and a low CTE. As a result, we fabricated a high-mobility short-channel OTFT array using a similar process to that for an array on conventional glass. The spin-coated OSC film on the nanopaper comprised large crystalline domains and the resulting TFT exhibited high mobility of up to 1 $cm^2\ V^{-1}\ s^{-1}$, almost hysteresis-free characteristics, and good operational and mechanical stability. We believe that these combined technologies of solution-based organic TFTs and low-cost and eco-friendly paper substrates are promising for use in future flexible electronics application such as flexible displays.

4. Experimental Section

Fabrication of Transparent Nanofibers Paper: Wood chips of Sitka spruce (*Picea sitchensis*) were bleached by the Wise method and alkali treatment.[49] A water suspension containig never-dried wood pulp was mechanically nanofibrillated using a high-pressure water jet system (Star Burst, HJP-25005E, Sugino Machine Co., Ltd.) equipped with a ball-collision chamber.[50] After the mechanical nanofibrillation, a cellulose nanofiber hydrogel was obtained (1 wt% fiber content). The nanofiber gel was cast onto a smooth acrylic plate and then oven dried at 50 °C for 1 day. After drying, an optically transparent nanopaper with a thickness of 20 μm was obtained.

Organic TFT Array: The bottom-contact OTFTs consisted of Mo gate electrodes, fluoro-based polymer gate dielectric layer (EPRIMA, AL-X6, Asahi Glass Co. Ltd., Japan), Au source/drain electrodes, and an organic semiconductor (OSC, lisiconS1200 Merck Chemicals Ltd.) film. Before fabrication of the OTFT array, 20-μm-thick transparent nanopaper was laminated on a glass substrate using a weak adhesive film (FixFilm, FujicopianCo., Japan) and the laminated nanopaper was heated in a vaccum oven at 100 °C for 1 h to remove undesirable air bubbles between the nanopaper and glass substrate. Then, the nanopaper was covered with a 2 μm-thick thermally cross-linkable olefin-type polymer (ZEOCOAT, Zeon Co., Japan). Mo gate electrodes with a thickness of 50 nm were sputtered at room temperature then patterned. A polymer gate dielectric layer was spin-coated under air at 2000 r.p.m. and then cured at 150 °C for 2 h for complete cross-linking after precuring treatment at 90 °C. The thickness of the dielectric was 300 nm. A 50-nm-thick Au source/drain electrode was deposited by e-beam deposition and patterned by wet etching using an etchant (Aurum-302, Kanto Chemical Co.). The fabricated array device was immersed in a thiol-based self-assembled monolayer (SAM) solution for the surface modification of the Au contact, which was followed by brief UV/O_3 exposure. Then, the substrate was rinsed with pure isopropanol solution and dried with a nitrogen gas stream. The OSC solution (2 wt% mesitylene solution) was spin-coated at room temperature and immediately cured at 100 °C for 30 min on a hot plate under air condition. Finally, the 20-μm-thick transparent nanopaper integrated with the OTFT array was peeled off from the support glass without any fracturing or cracks.

Characterization: Scanning electron microscopy (SEM, Hitachi S-4500) was used to characterize the surface morphology of the nanopaper. SEM samples were prepared by depositing a thin layer of Pt onto the nanopaper. The optical transmittance of the nanopaper was measured by spectrophotometer (Shimadzu UV-3100). To evaluate the thermal durability of the nanopaper, bare nanopaper sheet was cured at 100, 150, and 180 °C for 1 h on a hot plate. The morphology and crystalline structure of the OSC films were characterized by digital microscopy (Keyence, VHX-2000), cross-polarized optical microscopy (Olympus, BX51TRF), and atomic force microscopy (AFM, Digital Instruments Dimension 3100). The contact angle of the gate dielectric was measured by using a dispense system (Kyowa Interface Science Co., Ltd DropMaster DMC-MC3). Low-frequency (20 Hz) capacitance-voltage characteristics were used to estimate the gate capacitance (12.1 nF cm^{-2}), and this value was used for mobility calculation. The fabricated OTFT arrays were electrically characterized under a dark condition in air using a Keithley 4200-SCS semiconductor parameter analyzer and a semi-auto proving system (SUSS, PA200 BlueRay).

Supporting Information

Supporting Information is available from the Wiley Online Library or from the author.

Acknowledgements

The authors acknowledge Asahi Glass Co., LTD. for providing the fluoropolymer dielectric and for various discussions.

Received: August 29, 2013
Revised: September 21, 2013
Published online: November 19, 2013

[1] H. E. A. Huitema, G. H. Gelinck, J. B. P. H. Putten, K. E. Kuijk, K. M. Hart, E. Cantatore, P. T. Herwig, A. J. J. M. Breemen, D. M. de Leeuw, *Nature* **2001**, *414*, 599.
[2] M. Mizukami, N. Hirohata, T. Iseki, K. Ohtawara, T. Tada, S. Yagyu, T. Abe, T. Suzuki, Y. Fujisaki, Y. Inoue, S. Tokito, T. Kurita, *IEEE Electron Device Lett.* **2006**, *27*, 249.
[3] M. Noda, N. Kobayashi, M. Katsuhara, A. Yumoto, S. Ushikura, R. Yasuda, N. Hirai, G. Yukawa, I. Yagi, K. Nomoto, T. Urabe, *J. Soc. Info. Display* **2011**, *19*, 316.
[4] R. Matsubara, Y. Harada, K. Hatta, T. Yamamoto, M. Takei, M. Ishizaki, M. Matsumura, K. Ota, M. Ito, *Tech. Dig. SID.* **2012**, *32*, 419.
[5] D. Tobjork, R. Osterbacka, *Adv. Mater.* **2011**, *23*, 1935.
[6] P. Andersson, D. Nilsson, P. O. Svensson, M. Chen, A. Malmstrom, T. Remonen, T. Kugler, M. Berggren, *Adv. Mater.* **2002**, *14*, 1460.
[7] R. Martins, P. Barquinha, L. Pereira, N. Correia, G. Goncalves, I. Ferreira, E. Fortunato, *Appl. Phys. Lett.* **2008**, *93*, 203501.
[8] A. C. Siegel, S. T. Phillips, M. D. Dickey, N. Lu, Z. Suo, G. M. Whitesides, *Adv. Funct. Mater.* **2010**, *20*, 28.
[9] D. Y. Kim, A. J. Steckl, *ACS Appl. Mater. Interfaces* **2010**, *2*, 3318.
[10] L. Hu, H. Wu, F. L. Mantia, Y. Yang, Y. Cui, *ACS Nano* **2010**, *4*, 5843.
[11] M. C. Barr, J. A. Rowehl, R. R. Lunt, J. Xu, A. Wang, C. M. Boyce, S. G. Im, V. Bulovic´, K. K. Gleason, *Adv. Mater.* **2011**, *23*, 3500.
[12] A. D. Mazzeo, W. B. Kalb, L. Chan, M. G. Killian, J.-F. Bloch, B. A. Mazzeo, G. M. Whitesides, *Adv. Mater.* **2012**, *24*, 2850.
[13] R. A. Street, *Adv. Mater.* **2009**, *21*, 2007.
[14] T. Tsukada, *Technology and Applications of Amorphous Silicon* (Ed: R. A. Street), Springer-Verlag, Germany **2000**.
[15] E. Fortunato, N. Correia, P. Barquinha, L. Pereira, G. Gonçalves, R. Martins, *IEEE Electron Devices Lett.* **2008**, *29*, 988.
[16] W. Lim, E. A. Douglas, D. P. Norton, S. J. Pearton, F. Ren, Y.-W. Heo, S. Y. Son, J. H. Yuh, *Appl. Phys. Lett.* **2010**, *96*, 053510.
[17] R. Martins, A. Ahnood, N. Correia, L. Pereira, R. Barros, P. Barquinha, R. Costa, I. Ferreira, A. Nathan, E. Fortunato, *Adv. Funct. Mater.* **2013**, *23*, 2153.
[18] A. Dodabalapur, *Mater. Today* **2004**, *9*, 24.
[19] Y. H. Kim, D. G. Moon, J. I. Han, *IEEE Electron Devices Lett.* **2004**, *25*, 702.
[20] F. Eder, H. Klauk, M. Halik, U. Zschieschang, G. Schmid, C. Dehm, *Appl. Phys. Lett.* **2004**, *84*, 2673.
[21] U. Zschieschang, T. Yamamoto, K. Takimiya, H. Kuwabara, M. Ikeda, T. Sekitani, T. Someya, H. Klauk, *Adv. Mater.* **2011**, *23*, 654.
[22] Y. Li, C. Liu, Y. Xu, T. Minari, P. Darmawan, K. Tsukagoshi, *Org. Electron.* **2012**, *13*, 815819.
[23] M. Nogi, S. Iwamoto, A. N. Nakagaito, H. Yano, *Adv. Mater.* **2009**, *21*, 1595.
[24] C. S. Kim, S. Lee, E. D. Gomez, J. E. Anthony, Y.-L. Loo, *Appl. Phys. Lett.* **2008**, *93*, 103302.
[25] J. Huang, H. Zhu, Y. Chen, C. Preston, K. Rohrbach, J. Cumings, L. Hu, *ACS Nano.* **2013**, *7*, 2106.
[26] H. Fukuzumi, T. Saito, Y. Okita, A. Isogai, *Polym. Degrad. Stab.* **2010**, *95*, 1502.
[27] Y. Fujisaki, Y. Nakajima, D. Kumaki, T. Yamamoto, S. Tokito, T. Kono, J. Nishida, Y. Yamashita, *Appl. Phys. Lett.* **2010**, *97*, 133303.
[28] J. Soeda, Y. Hirose, M. Yamagishi, A. Nakao, T. Uemura, K. Nakayama, M. Uno, Y. Nakazawa, K. Takimiya, J. Takeya, *Adv. Mater.* **2011**, *23*, 3309.
[29] H. Li, B. C. Tee, J. J. Cha, Y. Cui, J. W. Chung, S. Y. Lee, Z. Bao, *J. Am. Chem. Soc.* **2012**, *134*, 2760.
[30] J. Jang, S. Nam, K. Im, J. Hur, S. N. Cha, J. Kim, H. B. Son, H. Suh, M. A. Loth, J. E. Anthony, J.-J. Park, C. E. Park, J. M. Kim, K. Kim, *Adv. Funct. Mater.* **2012**, *22*, 1005.
[31] T. Lee, C. A. Landis, B. M. Dhar, B. J. Jung, J. Sun, A. Sarjeant, H.-J. Lee, H. E. Katz, *J. Am. Chem. Soc.* **2009**, *131*, 1692.
[32] J. Veres, S. D. Ogier, S. W. Leeming, D. C. Cupertino, S. M. Khaffaf, *Adv. Funct. Mater.* **2003**, *13*, 199.
[33] M.-H. Yoon, C. Kim, A. Facchetti, T. J. Marks, *J. Am. Chem. Soc.* **2006**, *128*, 12851.
[34] T. Umeda, D. Kumaki, S. Tokito, *Org. Electron.* **2008**, *9*, 545.
[35] M. P. Walser, W. L. Kalb, T. Mathis, T. J. Brenner, B. Batlogg, *Appl. Phys. Lett.* **2009**, *94*, 053303.
[36] G. Lloyd, T. Backlund, P. Brookes, L. W. Tan, P. Wierzchowiec, J.-Y. Lee, S. Bain, M. James, J. Canisius, S. Tierney, K. Kawamata, T. Wakimoto, *Proc. IDW.* **2010**, *10*, 469.
[37] S. E. Fritz, T. W. Kelley, C. D. Frisbie, *J. Phys. Chem. B* **2005**, *109*, 10574.
[38] N. B. Ukah, J. Granstrom, R. R. Sanganna Gari, G. M. King, S. Guha, *Appl. Phys. Lett.* **2011**, *99*, 24330.
[39] Y. Fujisaki, Y. Nakajima, T. Takei, H. Fukagawa, T. Yamamoto, H. Fujikake, *IEEE Trans. Electron Devices* **2012**, *59*, 3442.
[40] S. H. Kim, S. Nam, J. Jang, K. Hong, C. Yang, D. S. Chung, C. E. Park, W-S. Choi, *J. Appl. Phys.* **2009**, *105*, 104509.
[41] H. Fukuzumi, T. Saito, T. Iwata, Y. Kumamoto, A. Isogai, *Biomacromolecules* **2009**, *10*, 162.
[42] I. S. Bayer, D. Fragouli, A. Attanasio, B. Sorce, G. Bertoni, R. Brescia, R. D. Corato, T. Pellegrino, M. Kalyva, S. Sabella, P. P. Pompa, R. Cingolani, A. Athanassiou, *ACS Appl. Mater. Interfaces* **2011**, *3*, 4024.
[43] X. Tang, S. Nan, T. Wang, Y. Chen, F. Yu, G. Zhang, M. Pei, *RSC Adv.* **2013**, *3*, 15571.
[44] A. C. Glavan, R. V. Martinez, A. B. Subramaniam, H. J. Yoon, R. M. D. Nunes, H. Lange, M. M. Thuo, G. M. Whitesides, *Adv. Funct. Mater.*, DOI: 10.1002/adfm.201300780.
[45] R. Hausermann, B. Batlogg, *Appl. Phys. Lett.* **2011**, *99*, 083303.
[46] H. Gleskova, S. Wagner, W. Soboyejo, Z. Suo, *J. Appl. Phys.* **2002**, *92*, 6224.
[47] T. Sekitani, U. Zschieschang, H. Klauk, T. Someya, *Nat. Mater.* **2010**, *10*, 1015.
[48] Y. Zhou, C. F-Hernandez, T. M. Khan, J-C. Liu, J. Hsu, J. W. Shim, A. Dindar, J. P. Youngblood, R. J. Moon, B. Kippelen, *Sci. Rep.* **2013**, *3*, 1536.
[49] K. Abe, S. Iwamoto, H. Yano, *Biomacromolecules* **2007**, *8*, 3276.
[50] M. Nogi, C. Kim, T. Sugahara, T. Inui, T. Takahashi, K. Suganuma, *Appl. Phys. Lett.* **2013**, *102*, 181911.